MINISTRY OF EDUCATION AND TRAINING

VIETNAM ACADEMY OF SCIENCE AND TECHNOLOGY

GRADUATE UNIVERSITY OF SCIENCE AND TECHNOLOGY

NGUYEN SY HIEP

METHOD FOR GENERATING ELASTICITY AND VISCOSITY IMAGES OF DISEASED SOFT TISSUE USING NOISE PROCESSING TECHNIQUES

SUMMARY OF DOCTORAL DISSERTATION IN COMPUTER SCIENCE

Specialty: Information Systems

Code: 9 48 01 04

Hanoi - 2026

The dissertation is completed at: Graduate University of Science and Technology, Vietnam Academy of Science and Technology

Scientific supervisors:

1. Supervisor: ....

2. Supervisor: ....

Reviewer 1: ....

Reviewer 2: ....

Reviewer 3: ....

The dissertation will be examined by Examination Board of Graduate University of Science and Technology, Vietnam Academy of Science and Technology at………………….. (time, date, year…)

This dissertation can be found at:

1) Graduate University of Science and Technology Library
2) National Library of Vietnam

INTRODUCTION

Cancer is currently one of the leading causes of mortality worldwide. According to the GLOBOCAN 2022 report of the International Agency for Research on Cancer (IARC), there are approximately 20 million new cases and nearly 10 million cancer-related deaths each year. In Vietnam, the year 2022 recorded approximately 180,480 new cases and 120,184 deaths. Numerous studies indicate that cancer risk is closely associated with environmental and lifestyle factors such as tobacco smoking, air pollution, obesity, and physical inactivity. Notably, the majority of cancer cases are detected only at advanced stages, which complicates treatment and substantially increases healthcare costs. Therefore, early detection is critically important for improving treatment outcomes and patient survival rates.

Currently, several diagnostic imaging techniques are employed in medicine, including ultrasound, X-ray, computed tomography (CT), magnetic resonance imaging (MRI), positron emission tomography-CT (PET-CT), and single photon emission computed tomography-CT (SPECT-CT). However, these methods still suffer from limitations such as high cost, lengthy examination times, or exposure to ionising radiation. In this context, ultrasound elastography has emerged as a promising solution, offering the advantages of being non-invasive, safe, low-cost, fast, and repeatable. In particular, elastography provides information on tissue stiffness and viscosity, which effectively supports the early detection of diseases such as breast cancer, thyroid cancer, prostate cancer, and liver fibrosis.

Despite these advantages, ultrasound elastography still faces several challenges, including random noise, speckle noise, reflection noise, and depth-dependent attenuation of shear-wave energy, all of which degrade image quality and the accuracy of mechanical parameter estimation. Motivated by these practical considerations, this dissertation adopts the topic: "METHOD FOR GENERATING ELASTICITY AND VISCOSITY IMAGES OF DISEASED SOFT TISSUE USING NOISE PROCESSING TECHNIQUES".

The objective of this dissertation is to develop methods and algorithmic models that improve the accuracy of estimating soft-tissue elasticity and viscosity from the shear-wave velocity field, while simultaneously enhancing the quality of viscoelastic images in inhomogeneous tissue environments. The research object is the shear-wave velocity signal acquired in ultrasound elastography. The dissertation employs numerical simulation combined with signal processing. The finite-difference time-domain (FDTD) method is used to simulate shear-wave propagation in biological tissue, while algebraic Helmholtz inversion (AHI) is applied to estimate the complex shear modulus of tissue. Least-mean-squares (LMS), median, and directional filters are integrated to address the characteristic noise types in ultrasound imaging.

The main contributions of the dissertation are: (1) proposing a method that combines noise filtering techniques to improve the quality of elasticity and viscosity images in inhomogeneous tissue environments; and (2) proposing a multi-point excitation model to enhance image quality in deep-tissue regions, where shear-wave energy is significantly attenuated.

CHAPTER 1: OVERVIEW OF ULTRASOUND ELASTOGRAPHY

1.1. Background and significance of the topic

Over recent decades, the rising prevalence of cancer has highlighted the need for non-invasive, safe diagnostic techniques capable of early detection. At present, methods such as X-ray, CT, MRI, PET-CT, and SPECT-CT are widely used in diagnostic imaging. Nevertheless, these techniques are still subject to limitations including ionising radiation, high cost, or lengthy acquisition times.

To overcome these limitations, ultrasound elastography has attracted growing interest owing to its safety, non-invasive nature, low cost, and real-time imaging capability. In particular, this technique not only provides morphological information but also enables the assessment of tissue elasticity and viscosity, effectively supporting the differentiation between healthy and diseased tissue.

Figure 1.1: Mammography and X-ray mammographic image

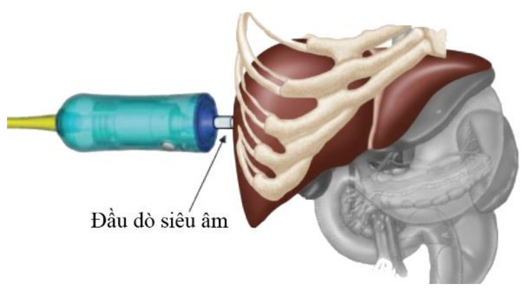

Figure 1.2: Fibroscan technique for liver fibrosis examination

1.2. Theoretical basis of ultrasound elastography

From traditional palpation to modern clinical practice, tissue stiffness remains an important indicator in disease diagnosis. However, palpation depends heavily on the physician's experience and is inherently subjective.

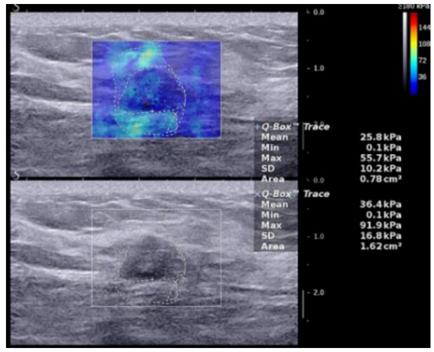

Figure 1.3: Ultrasound elastography image of a female breast

Ultrasound elastography encodes tissue stiffness using a colour scale (from blue to red), allowing intuitive visualisation of stiffness information, which is quantified by Young's modulus (Pa), an attribute that B-mode ultrasound cannot provide.

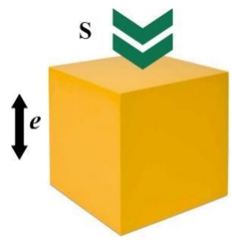

Figure 1.4: Strain under applied compressive force

$$E = \frac{s}{e} \tag{1.1}$$

Where: s is the applied compressive stress, e is the strain of the tissue, and E is Young's modulus (Figure 1.4). Numerous studies have demonstrated the value of elastography in distinguishing between malignant and benign lesions. The stiffness of malignant tissue is significantly greater than that of benign tumours [43].

Table 1.1: Stiffness of selected soft-tissue types

Type of soft tissue	Young's modulus (E, kPa)	Density (ρ, kg/m³)
Breast		1000 ± 8%
Normal fat	18 – 24	
Normal glandular	28 – 66	
Fibrous tissue	96 – 244	
Carcinoma	22 – 560	

1.3. Challenges affecting the quality of ultrasound elastography images

In ultrasound elastography, the mechanical properties of tissue are inferred from the shear-wave propagation velocity rather than from the amplitude of ultrasonic echoes as in B-mode. However, the signals used to estimate shear-wave velocity may be affected by various types of noise and distortion, which degrade the accuracy of elastography images and the reliability of quantitative parameters. These noise sources affect not only image quality but also the reliability of quantitative parameters, particularly in deep-tissue regions that are clinically significant. The specific challenges are analysed below according to each type of noise.

1.4. Current research status

International research

In reality, biological tissue exhibits viscoelastic behaviour; therefore, estimating stiffness alone is insufficient to accurately characterise the mechanical properties of diseased tissue. Recent studies have shown that simultaneously estimating elasticity and viscosity provides more effective differentiation between healthy and diseased tissue, particularly in conditions such as cancer, liver fibrosis, and hepatic steatosis [63-65]. The algebraic Helmholtz inversion (AHI) method allows reliable simultaneous estimation of both parameters, thereby improving the reconstruction of the complex shear modulus (CSM) in inhomogeneous tissue [66-69].

Conventional ultrasound elastography techniques typically involve two steps: generating shear waves by acoustic radiation force (ARF) or mechanical excitation, then measuring the mechanical response of the tissue to estimate viscoelastic parameters [35, 70-75]. In 2007, Zheng et al. employed a Kalman filter to analyse shear-wave motion and estimate the dispersion characteristics of tissue [76]; however, this method demands substantial computational effort and did not account for measurement noise. In the study by Hengzhao et al. [35], elasticity and viscosity were determined from shear-wave propagation velocity and attenuation coefficients using a two-dimensional Fourier transform, but the analysis was limited to homogeneous media and did not consider acquisition noise.

Deffieux et al. [78] investigated the effects of reflected waves in tumour-containing media and applied a directional filter to improve elastography image quality; nevertheless, random noise and speckle noise were not considered. Njeh et al. [79] proposed the SMU algorithm, which combines SRAD, median filtering, and unsharp masking to reduce speckle noise and enhance breast ultrasound image quality. Overall, international research has achieved considerable progress in estimating viscoelastic properties of tissue; however, simultaneous suppression of multiple noise types and image quality improvement in inhomogeneous tissue environments remain open challenges.

Domestic research

In Vietnam, research on signal processing in ultrasound elastography has attracted growing attention in recent years. Pham-Thi et al. [66] proposed a method combining AHI and an LMS filter to estimate the 2D complex shear modulus in noisy environments, leading to improved viscoelastic image quality. Quang-Huy et al. [67] further exploited AHI in combination with bandpass filtering to reconstruct viscoelastic images under various noise conditions. More recently, Tran et al. [89] proposed a multi-frequency combination method together with the LMS/AHI algorithm to enhance estimation in complex signal environments. These domestic studies indicate that integrated approaches combining noise processing with complex shear modulus estimation are receiving increasing interest; nevertheless, the simultaneous suppression of multiple noise types and the improvement of image quality in deep-tissue regions remain open challenges.

1.5. Conclusion of Chapter 1

In this chapter, the candidate has presented an overview of ultrasound elastography, the theoretical basis of the complex shear modulus (CSM), and the factors affecting elastography image quality. Ultrasound elastography is a non-invasive, safe, and low-cost technique that enables the assessment of soft-tissue elasticity and viscosity, effectively supporting the detection and classification of pathologies such as cancer and liver fibrosis. The survey results show that elastography image quality is affected by random noise, speckle noise, reflection noise, and depth-dependent shear-wave attenuation, all of which reduce the accuracy of CSM estimation.

Various noise processing methods and shear-wave generation techniques have been investigated to improve image quality. However, the effective combination of noise processing techniques and the enhancement of image quality in inhomogeneous tissue environments remain open challenges and constitute the research direction pursued in the following chapters of this dissertation.

CHAPTER 2: COMBINED NOISE-FILTERING METHOD FOR IMPROVING VISCOELASTIC IMAGE QUALITY

In this chapter, the candidate presents the principles of shear-wave generation and propagation in inhomogeneous soft tissue and constructs a simulation model based on the FDTD method. The AHI method is employed to estimate the complex shear modulus (CSM), in combination with LMS, median, and directional filters to improve the quality of 2D viscoelastic images. The results comprise images of the spatial distribution of elasticity and viscosity after noise processing, which are quantitatively evaluated using the RMSE index. The results of this chapter have been published in [CT2], [CT4], [CT5], [CT6], and [CT7].

2.1. Shear-wave propagation and acquisition

Shear-wave propagation in tissue

Shear waves can be generated using focused or unfocused acoustic beams, such as the comb-push ultrasound shear elastography (CUSE) technique; however, these methods require high-power ultrasound systems with complex configurations and high cost. Therefore, in this study, the candidate adopts mechanical shear-wave generation using a vibrating needle operating in the 50-500 Hz range, owing to its flexible adjustability and ease of implementation. Shear waves propagate through tissue and undergo reflection at the boundary between healthy tissue and tumours. The velocity signals acquired by Doppler ultrasound are typically affected by various noise types; therefore, noise reduction to improve image quality is a key objective of this research.

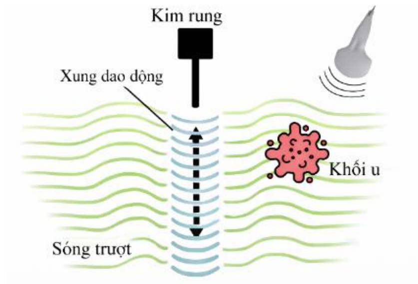

Figure 2.1: Generation and propagation of shear waves in tissue

Shear-wave acquisition

Doppler pulses are used to track tissue motion induced by shear waves, from which the propagation velocity is estimated [80-82]. In the measurement system, an ultrasound transducer transmits and receives the reflected signals from tissue using pulsed Doppler. The received echo signals are then processed by a phase-shift-based Doppler estimator to determine the oscillation velocity of tissue particles. The acquired velocity field reflects the shear-wave propagation in tissue and serves as the basis for estimating the elasticity and viscosity of soft tissue.

Shear-wave propagation model using the FDTD method

In tissue biomechanics, classical viscoelastic models commonly used to describe the mechanical properties of soft tissue include the Kelvin–Voigt, Maxwell, and Standard Linear Solid (SLS) models.

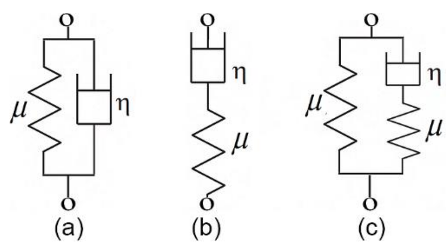

Figure 2.2: Kelvin-Voigt (a), Maxwell (b), and SLS (c) models

In Chapters 2 and 3, the candidate uses the Kelvin-Voigt model to characterise the elastic and viscous behaviour of tissue. The Kelvin-Voigt equation is expressed as in (2.1) [84-88].

$$G(x, y, \omega) = \mu(x, y) + i\omega\eta(x, y) \tag{2.1}$$

Where G is the complex shear modulus (CSM), $\mu(x, y)$ is the elasticity, and $\eta(x, y)$ is the viscosity at spatial position (x, y). The vibrating needle is located at position (0, 0). According to the Kelvin-Voigt equation above, the CSM depends on the angular frequency ω of the oscillation produced by the vibrating needle.

The relationship between particle velocity and the components of the strain tensor is established through equations (2.2), (2.3), and (2.4).

$$v_z^{n+1}\Big|_{i,j} = v_z^{n}\Big|_{i,j} + \frac{\Delta_t}{\rho\Delta_x}\left(\sigma_{zx}^{n+\frac{1}{2}}\Big|_{i+\frac{1}{2},j} - \sigma_{zx}^{n+\frac{1}{2}}\Big|_{i-\frac{1}{2},j}\right) + \frac{\Delta_t}{\rho\Delta_y}\left(\sigma_{zy}^{n+\frac{1}{2}}\Big|_{i+\frac{1}{2},j} - \sigma_{zy}^{n+\frac{1}{2}}\Big|_{i-\frac{1}{2},j}\right) \tag{2.5}$$

$$\sigma_{zx}^{n+1}\Big|_{i+\frac{1}{2},j} = \sigma_{zx}^{n-\frac{1}{2}}\Big|_{i+\frac{1}{2},j} + \frac{\mu\Delta_t}{\Delta_x}\left(v_z^{n+1}\Big|_{i+1,j} - v_z^{n+1}\Big|_{i,j}\right) + \frac{\eta}{\Delta_x}\left(v_z^{n+1}\Big|_{i+1,j} - v_z^{n+1}\Big|_{i,j}\right) - \frac{\eta}{\Delta_x}\left(v_z^{n}\Big|_{i+1,j} - v_z^{n}\Big|_{i,j}\right) \tag{2.6}$$

$$\sigma_{zy}^{n+1}\Big|_{i+\frac{1}{2},j} = \sigma_{zx}^{n-\frac{1}{2}}\Big|_{i+\frac{1}{2},j} + \frac{\mu\Delta_t}{\Delta_y}\left(v_z^{n+1}\Big|_{i+1,j} - v_z^{n+1}\Big|_{i,j}\right) + \frac{\eta}{\Delta_y}\left(v_z^{n+1}\Big|_{i+1,j} - v_z^{n+1}\Big|_{i,j}\right) - \frac{\eta}{\Delta_y}\left(v_z^{n}\Big|_{i+1,j} - v_z^{n}\Big|_{i,j}\right) \tag{2.7}$$

Δx and Δy denote the spacings between successive spatial positions along the X and Y axes, respectively. Δt is the sampling period (time step); i is the spatial index along the X axis; j is the spatial index along the Y axis; and n is the time-step index.

2.2. Proposed method

Signal-processing pipeline

To accurately reconstruct images of the mechanical properties of tissue from shear-wave velocity signals, the candidate constructs a signal-processing pipeline consisting of denoising and CSM estimation steps. The velocity signals acquired by the Doppler system contain the incident wave, the reflected wave, and random noise, and therefore require preprocessing before parameter estimation. First, the signal is transformed to the frequency domain using the DFT, and a directional filter is applied to suppress reflected waves. The signal is then transformed back to the time domain using the IDFT and further processed by an adaptive LMS filter to reduce random noise. The filtered signal is used in the AHI method to reconstruct 2D images of elasticity and viscosity. Finally, a median filter is applied to the CSM image to reduce speckle noise while preserving image edges. The filters are arranged in the order: directional, LMS, and median, so that each noise type is addressed separately while the physical structure of the shear wave is preserved. Consequently, the velocity information used for CSM estimation is retained, and the image quality is substantially improved.

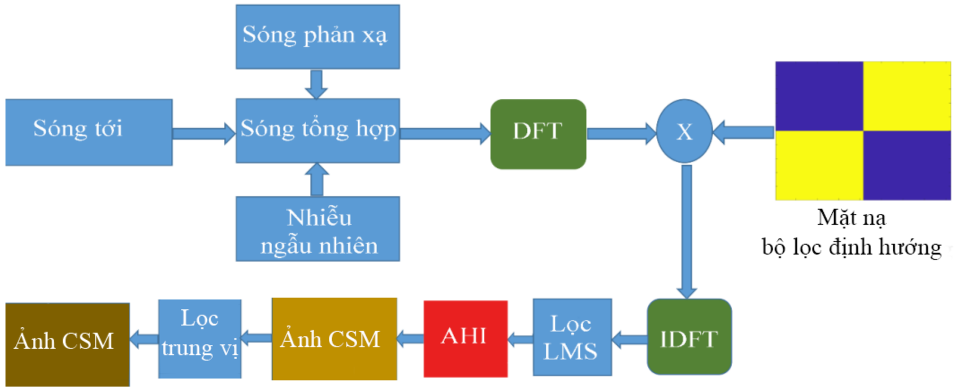

Figure 2.3: Signal-processing pipeline

Reflection-noise suppression using a directional filter

Reflected waves in inhomogeneous media that interfere with the incident wave are suppressed by a directional filter in the frequency domain, in which the DFT spectrum is multiplied by a mask that retains the incident wave components and removes the reflected wave components.

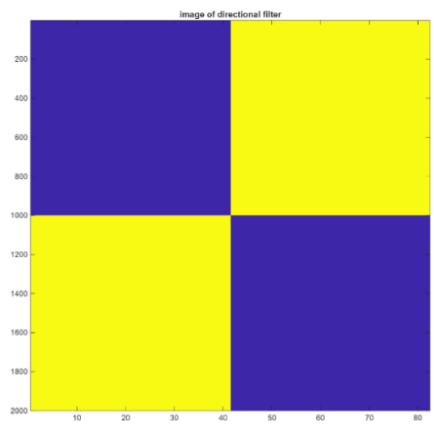

Figure 2.4: Directional filter mask

Random-noise suppression using an LMS filter

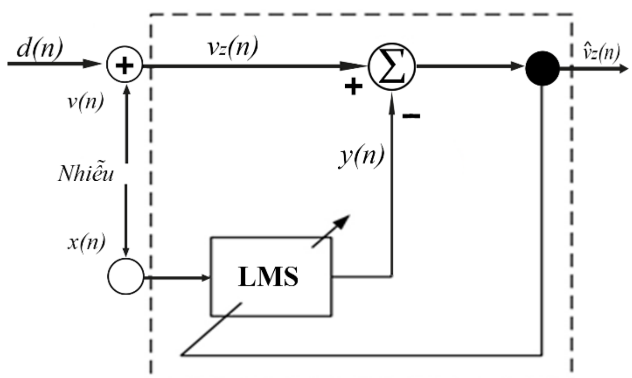

Figure 2.5: Operation of the LMS filter

LMS filtering algorithm

Step 1: Set the step size μ*, filter order L, and noise variance.

Step 2: Initialise the coefficients $w(n) = 0$.

Step 3: For $n = 0, 1, 2, 3, ...$

Compute the filter output: $y(n) = w(n) \cdot x(n)$

Compute the error: $e(n) = vz(n) - y(n)$

Update the coefficients: $w(n + 1) = w(n) + \mu^* \cdot e(n) \cdot x(n)$

Set the filtered signal: $vz(n) = e(n)$

Repeat until the end of the signal.

CSM estimation using algebraic Helmholtz inversion

After the shear-wave particle velocity has been filtered to remove reflection and random noise, the signal is used to estimate the CSM via the algebraic Helmholtz inversion [93]. Taking the time derivative of stress in equation (2.2) yields (2.8); equations (2.3) and (2.4) correspond to (2.9) and (2.10), respectively. Substituting (2.10) and (2.9) into (2.8) yields (2.11). Equation (2.11) shows that the right-hand side contains the CSM in the time domain together with the Laplacian operator, and is rewritten as (2.12). The Fourier transform of (2.12) yields the Helmholtz equation (2.13). Inverting equation (2.13) algebraically gives equation (2.14), which provides the CSM in the frequency domain. According to equation (2.1), the elasticity $\mu(x, y)$ and the viscosity $\eta(x, y)$ are the real and imaginary components of the CSM, respectively (equations 2.15 and 2.16).

Speckle-noise suppression using a median filter

Median filtering algorithm

Given an input image I of size $M \times N$, the median-filtering algorithm with a 3×3 window is implemented as follows:

Step 1: For each pixel $I(i, j)$ in the image (with $i \in [2, M - 1], j \in [2, N - 1]$), define a 3×3 neighbourhood window around that pixel.

Step 2: Extract all 9 pixel values within the window Wi,j: $W_{i,j} = \{I(i + r, j + c) \mid r \in \{-1, 0, 1\}, c \in \{-1, 0, 1\}\}$.

Step 3: Sort the 9 values in Wi,j in ascending order to obtain the sequence $S = \{s1, s2, ..., s9\}$ such that $s1 \leq s2 \leq ... \leq s9$.

Step 4: The median is the middle element: $\text{median}(W_{i,j}) = s5$.

Step 5: Assign the median value to the corresponding pixel in the output image: $I'(i, j) = \text{median}(W_{i,j})$.

Various window sizes were tested for the median filter, including 3×3, 5×5, and 7×7. The results show that the 3×3 window provides the best performance, achieving effective noise reduction while limiting over-smoothing, thereby preserving important edges and structures in the image.

2.3. Simulation scenario

To evaluate the effectiveness of the proposed method, a simulation of soft tissue measuring 80×80 mm containing a 30×30 mm tumour was constructed. The elasticity and viscosity parameters of healthy and diseased tissue are presented in Table 2.1, with a tissue density of 1000 kg/m³. Shear waves were generated by a vibrating needle oscillating at 150 Hz with an amplitude of 5 mm. To simulate realistic conditions, reflection and random noise were added to the acquired velocity signal.

Table 2.1: Elasticity and viscosity of tissue

Tissue type	Elasticity (Pa)	Viscosity (Pa·s)
Healthy tissue	6000	1.2
Diseased tissue	7000	1.5

2.4. Simulation results

Simulation results at SNR = 20 dB

Results after suppression of reflection and random noise

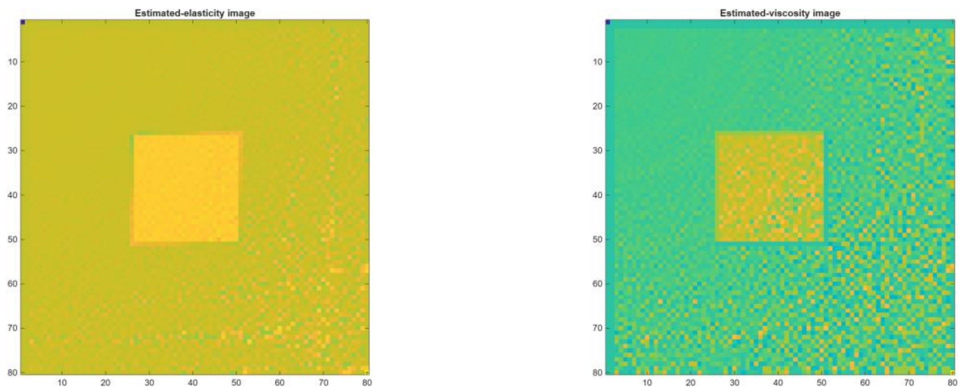

Figure 2.6: 2D images of elasticity and viscosity

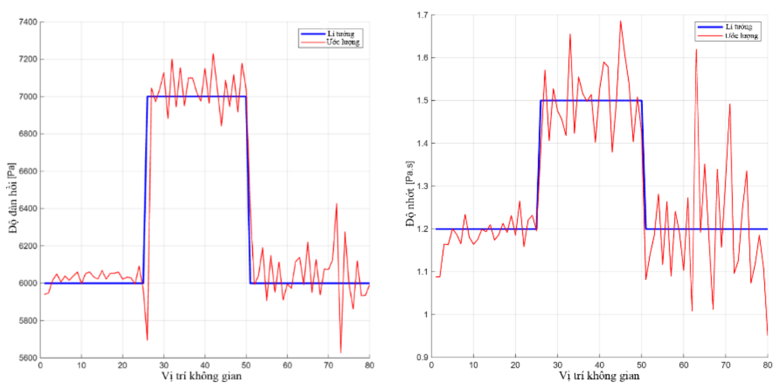

Figure 2.7: Elasticity and viscosity profiles along line 30

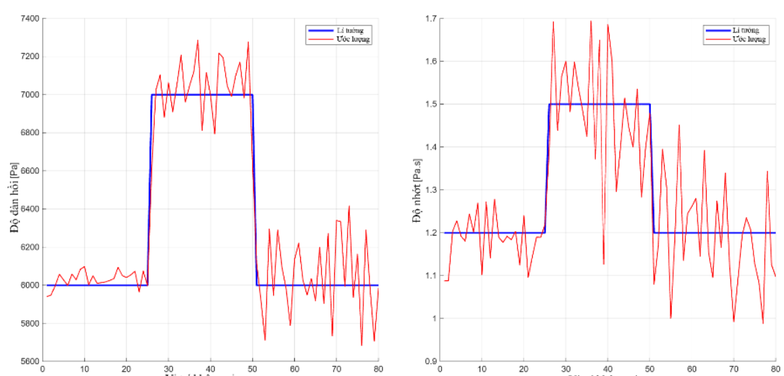

Figure 2.8: Elasticity and viscosity profiles along line 45

Results after speckle-noise suppression

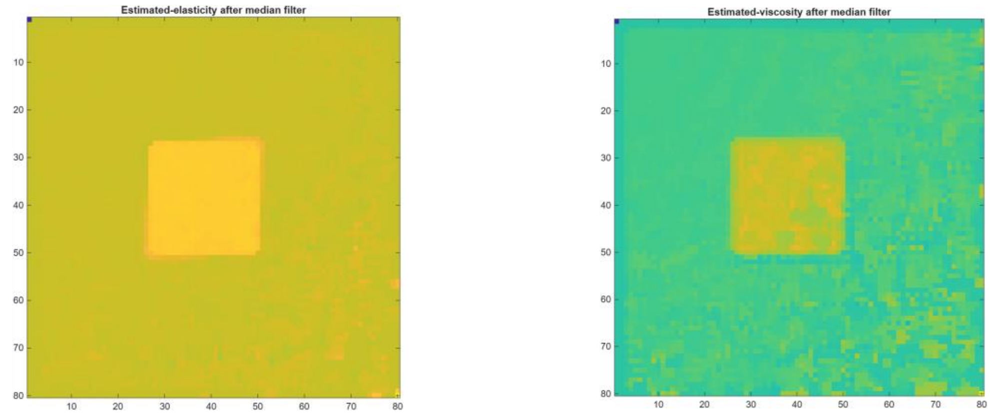

Figure 2.9: Estimated elasticity image after median filtering

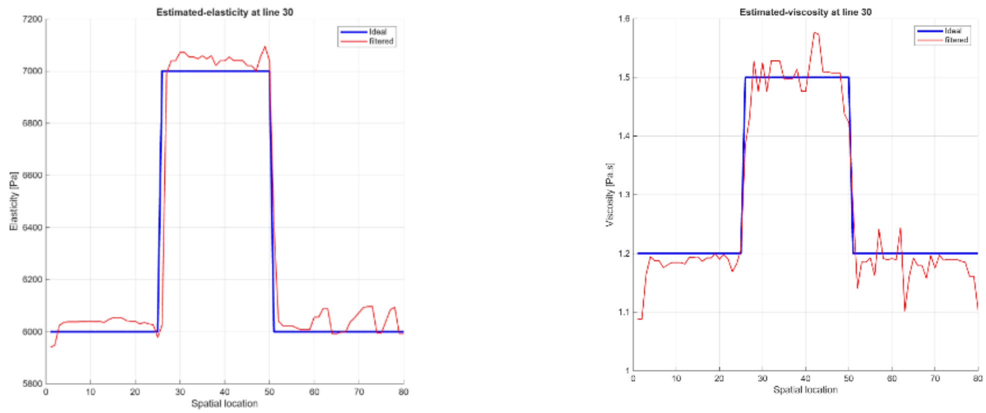

Figure 2.10: Elasticity and viscosity profiles along line 30 after speckle-noise filtering

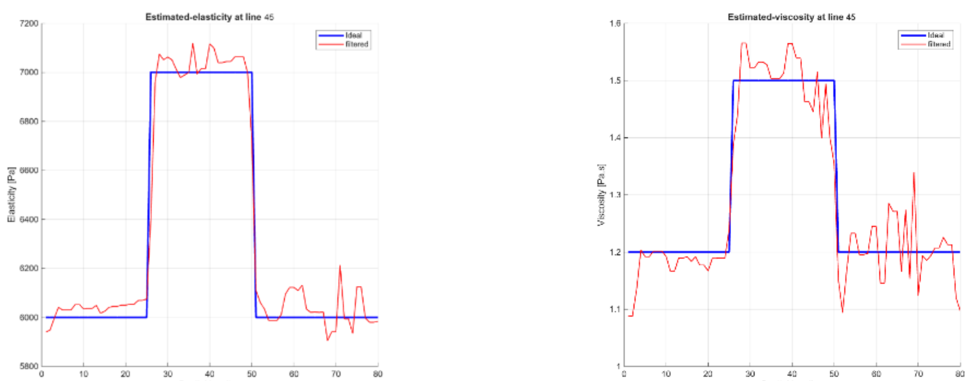

Figure 2.11: Elasticity and viscosity profiles along line 45 after speckle-noise filtering

Simulation results at SNR = 40 dB

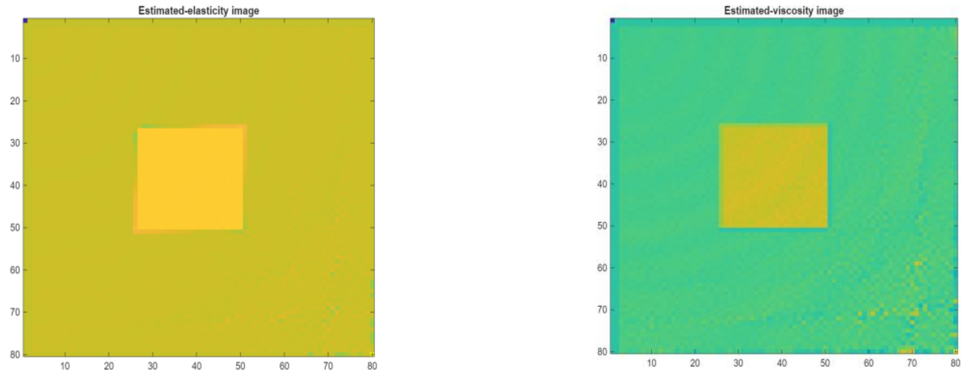

Figure 2.12: 2D elasticity and viscosity images

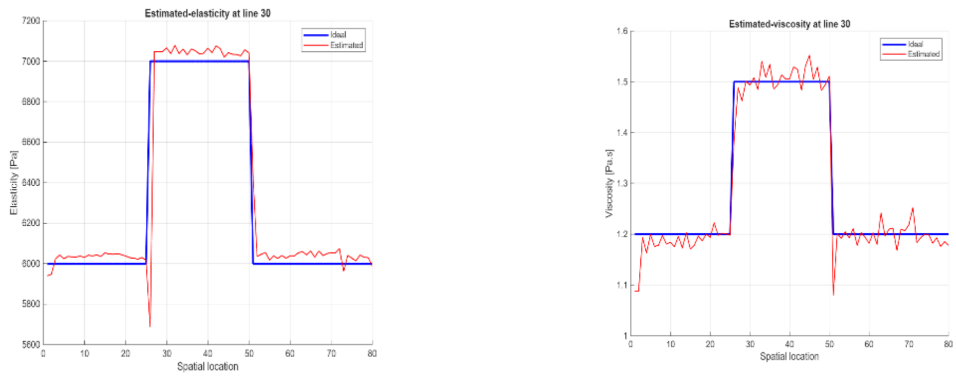

Figure 2.13: Elasticity and viscosity profiles along line 30

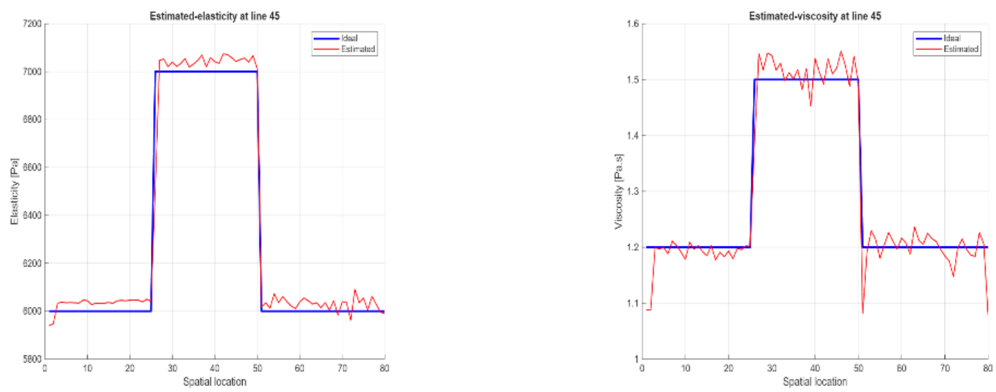

Figure 2.14: Elasticity and viscosity profiles along line 45

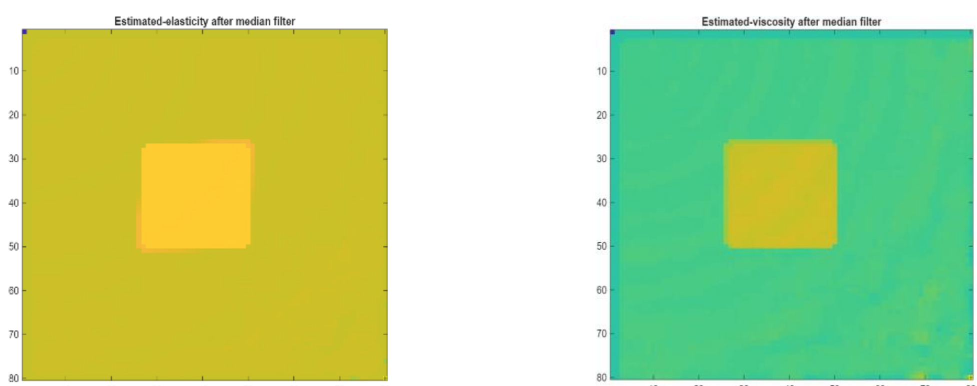

Figure 2.15: 2D elasticity and viscosity images after median filtering

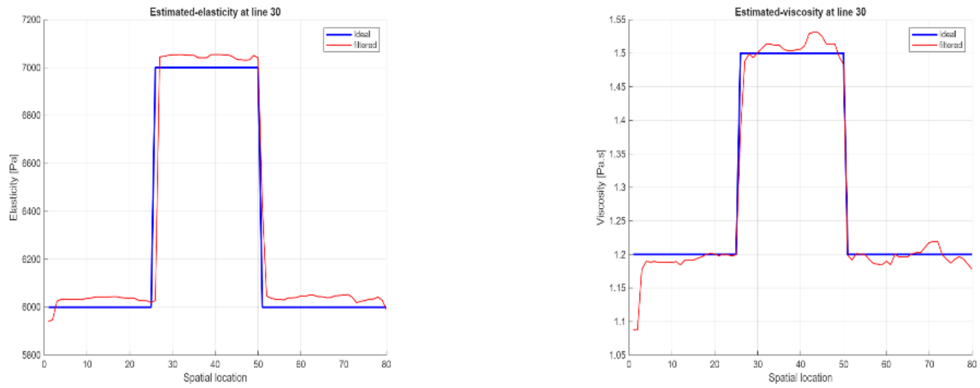

Figure 2.16: Elasticity and viscosity profiles along line 30 after speckle-noise filtering

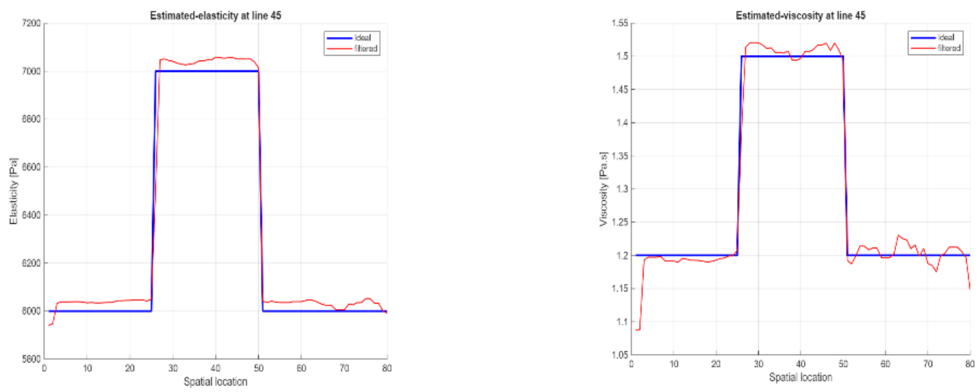

Figure 2.17: Elasticity and viscosity profiles along line 45 after speckle-noise filtering

The elasticity and viscosity images were successfully reconstructed from the velocity signals. By simulating different SNR levels, the results show that the post-filtering image quality is improved compared with the pre-filtering case. Although increasing the SNR substantially improves image quality and the accuracy of the estimated values, in experimental and clinical practice the SNR is limited by physical, instrumental, and biological factors. Therefore, the development of effective noise-processing and image-reconstruction methods is necessary to enhance CSM image quality under low- to moderate-SNR conditions.

2.5. Similarity-evaluation index: RMSE

The RMSE is a quantitative index measuring the difference between the estimated image and the ideal reference image. It is used to evaluate the quality of elasticity and viscosity images: the smaller the RMSE, the higher the estimation accuracy. However, RMSE reflects only the per-pixel mathematical error and does not separately capture contrast, image structure, or perceptual quality.

$$RMSE = \sqrt{\frac{1}{MN}\sum_{i=0}^{M-1}\sum_{j=0}^{N-1}[I(i,j)-K(i,j)]^2} \tag{2.13}$$

$$SNR = 10 * \log 10\left(\frac{Psignal}{Pnoise}\right) \tag{2.14}$$

For each SNR value, a corresponding RMSE value is obtained, where R_nh (1) and R_nh (2) denote the RMSE of the viscosity image before and after median filtering, and R_đh (1) and R_đh (2) denote the RMSE of the elasticity image before and after median filtering (Table 2.2).

Table 2.2: RMSE of elasticity and viscosity images as a function of SNR

SNR (dB)	R_nh (1)	R_nh (2)	R_đh (1)	R_đh (2)
20	0.130	0.064	197.2	105.0
26	0.122	0.060	202.1	105.3
30	0.118	0.055	193.3	103.4
32	0.111	0.052	182.4	102.4
34	0.106	0.047	169.0	101.6
36	0.095	0.041	159.2	100.2
37	0.087	0.037	144.9	99.8
38	0.078	0.032	132.6	98.6
39	0.065	0.026	120.4	98.4
40	0.055	0.023	112.0	98.3

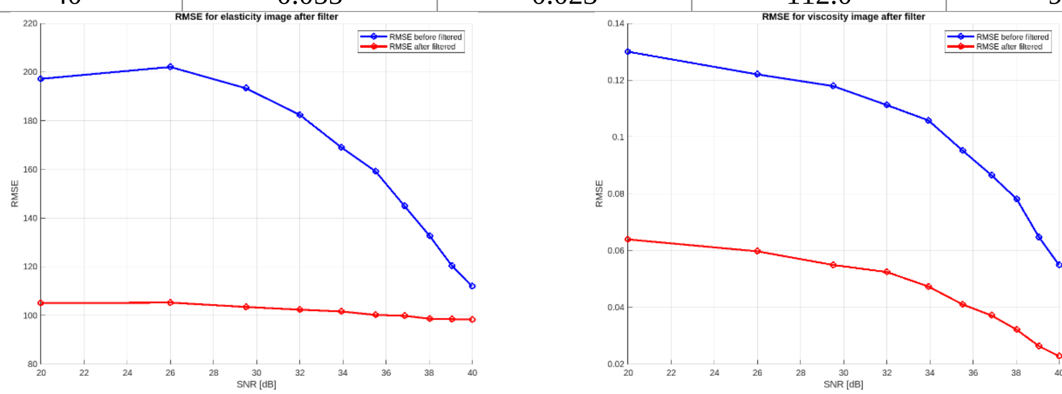

Figure 2.18: RMSE of elasticity and viscosity images before and after median filtering

2.6. Comparison with the study by Lipman et al.

Lipman et al. [100] proposed extending the directional filter from 2D to 3D and 4D to suppress reflection noise in the reconstruction of shear-wave-speed (SWS) images. Their results show that the 4D filter substantially improves image quality and reduces bias at the tumour boundary. However, the study addresses only reflection noise, without considering random noise or speckle noise; furthermore, the model assumes purely elastic tissue and does not account for tissue viscosity. In addition, the 4D method requires large computational resources and expensive hardware, which limits its practical applicability.

In contrast, this dissertation proposes the combined use of LMS, directional, and median filters to address multiple noise types in inhomogeneous tissue environments. Moreover, the proposed method estimates not only elasticity but also viscosity through the complex shear modulus (CSM), providing a more comprehensive characterisation of the mechanical properties of biological tissue. The effectiveness of the method is quantitatively assessed using the RMSE index, thereby improving accuracy and applicability in clinical diagnosis.

2.7. Conclusion of Chapter 2

In this chapter, the candidate proposes a method for estimating elasticity and viscosity images of tissue from shear-wave velocity using AHI, combined with LMS, median, and directional filters, in order to simultaneously suppress the principal noise types in ultrasound elastography. The results show that the image quality and the accuracy of mechanical-parameter estimation are clearly improved, as quantified by the RMSE index. The research results of this chapter have been published in [2], [4]–[7].

Nevertheless, noise remains higher in deep-tissue regions due to shear-wave energy attenuation, and the model considers only a simple square-shaped tumour. Therefore, Chapter 3 proposes a multi-point excitation method to improve image quality in deep-tissue regions and extends the simulation to more complex geometric structures.

CHAPTER 3: KELVIN-VOIGT MODEL WITH MULTI-POINT EXCITATION FOR VISCOELASTIC IMAGING IN DEEP TISSUE

3.1. Shear-wave generation and propagation

Figure 3.1: Shear-wave generation at two separate positions:

(a) excitation at position 1, (b) excitation at position 2

3.2. Proposed method

The velocity signal at each excitation position is first processed by an LMS filter to suppress random noise. Subsequently, elasticity and viscosity images are estimated using AHI. A median filter is then applied to reduce speckle noise and smooth the image. Finally, the images obtained from the two excitation positions are combined to produce a composite image of higher quality. Two signal-processing chains are executed independently for the two positions of the vibrating needle.

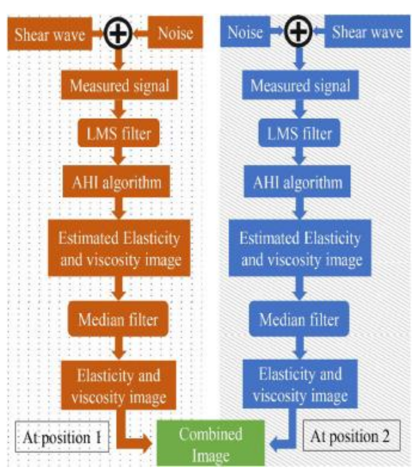

Figure 3.2: Procedure for viscoelastic image reconstruction

Image-combination algorithm from two excitation sources

Input: mu1_est1, eta_est1 — elasticity and viscosity images estimated from source 1 (size 80 × 80); mu1_est2, eta_est2 — elasticity and viscosity images estimated from source 2 (size 80 × 80). Output: mu1_est, eta_est — combined elasticity and viscosity images (size 80 × 80).

Procedure:

Step 1: Iterate over each pixel (i, j) in the 80 × 80 image domain:

For i = 1 to 80 do

For j = 1 to 80 do

Step 2: Check the horizontal position of the pixel and select the corresponding source:

If j ≤ 40 (left half): assign mu1_est(i, j) = mu1_est1(i, j) and eta_est(i, j) = eta_est1(i, j) (values from source 1).

Otherwise (right half, j > 40): assign mu1_est(i, j) = mu1_est2(i, j) and eta_est(i, j) = eta_est2(i, j) (values from source 2).

Step 3: Repeat for all pixels in the image, from (1, 1) to (80, 80).

Step 4: Output the combined image. The matrices mu1_est and eta_est are the elasticity and viscosity images combined from the two sources.

3.3. Simulation scenario and results

Simulation scenario

The FDTD method is used to simulate shear-wave propagation at two excitation positions in tissue of size 80 × 80 mm, with a vibrating needle at 150 Hz and 6 mm amplitude. This setup enables the assessment of the ability to distinguish healthy and diseased tissue (the latter being stiffer and more viscous) through viscoelastic parameters.

Table 3.1: Elasticity and viscosity of healthy and diseased tissue

Tissue type	Elasticity (Pa)	Viscosity (Pa·s)
Healthy tissue	6000	1.2
Tumour	9000	1.8

Simulation results at SNR = 29 dB

Source at position 1

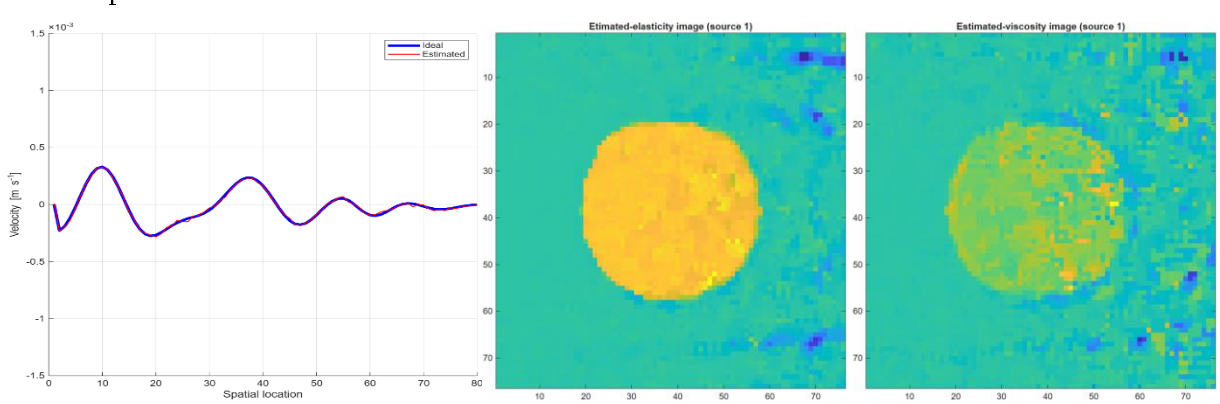

Figure 3.3: Estimated elasticity and viscosity images at position 1

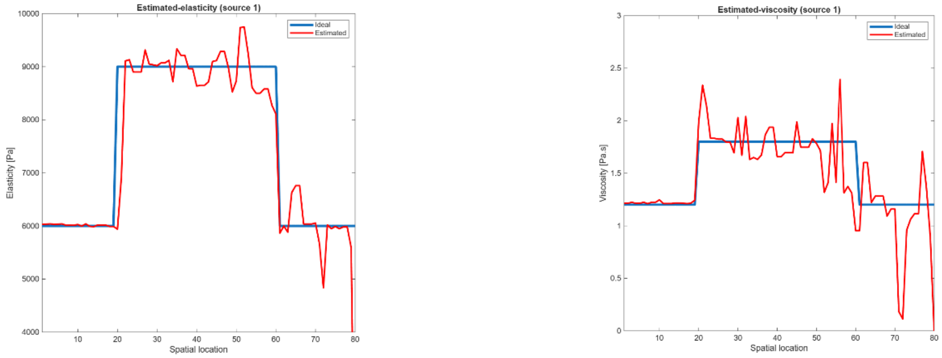

Figure 3.4: Elasticity and viscosity profiles along line 40

Source at position 2

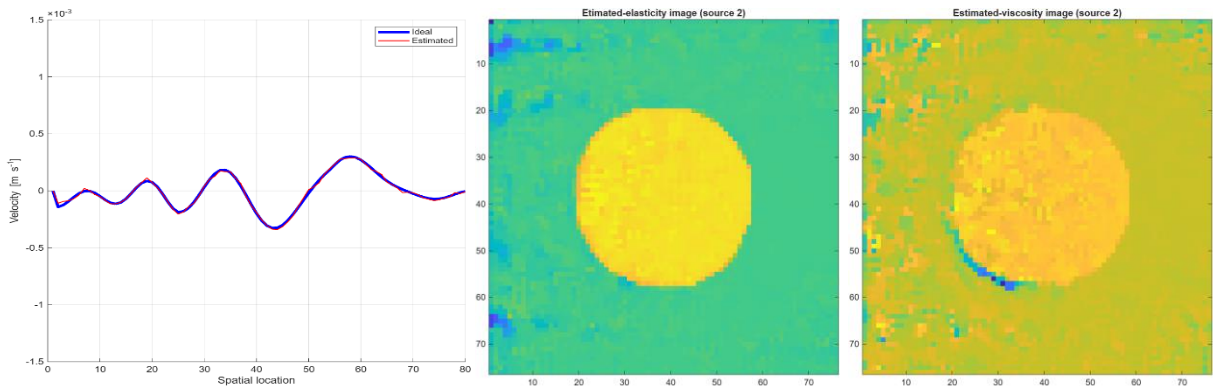

Figure 3.5: Estimated elasticity and viscosity images at position 2

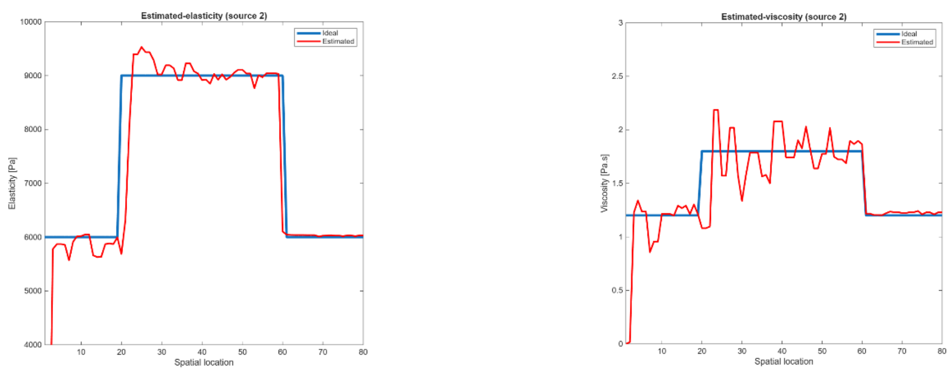

Figure 3.6: Elasticity and viscosity profiles along line 40

Combination of sources 1 and 2

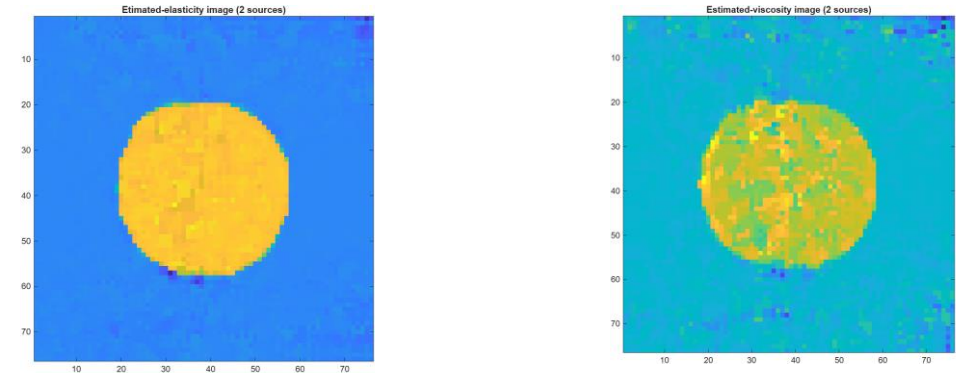

Figure 3.7: Combined elasticity and viscosity images

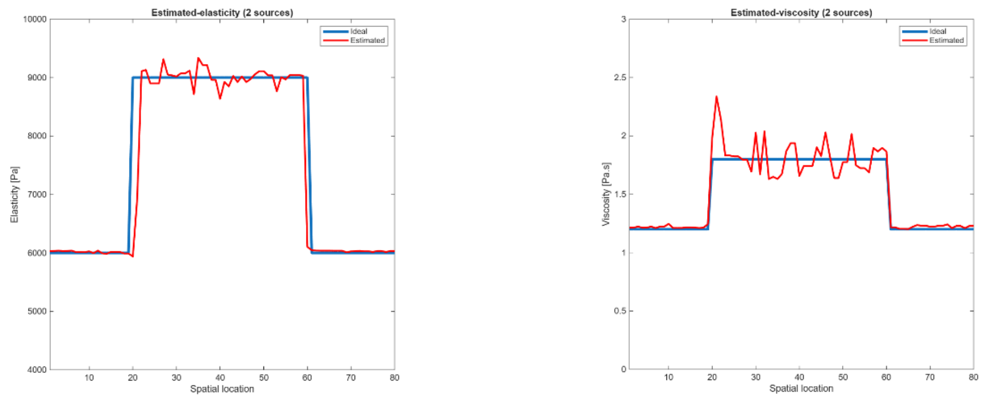

Figure 3.8: Combined elasticity and viscosity profiles along line 40

Simulation results at SNR = 19 dB

Source at position 1

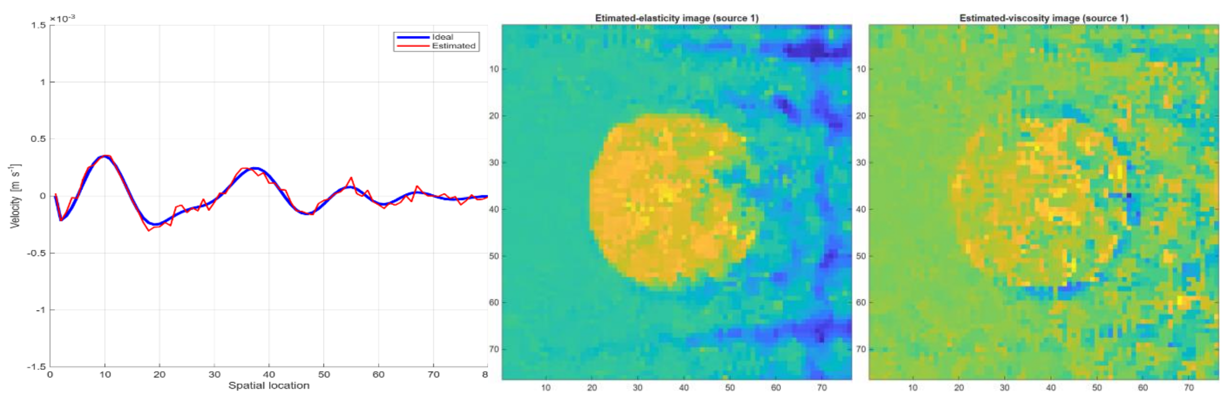

Figure 3.9: Estimated elasticity and viscosity images at position 1

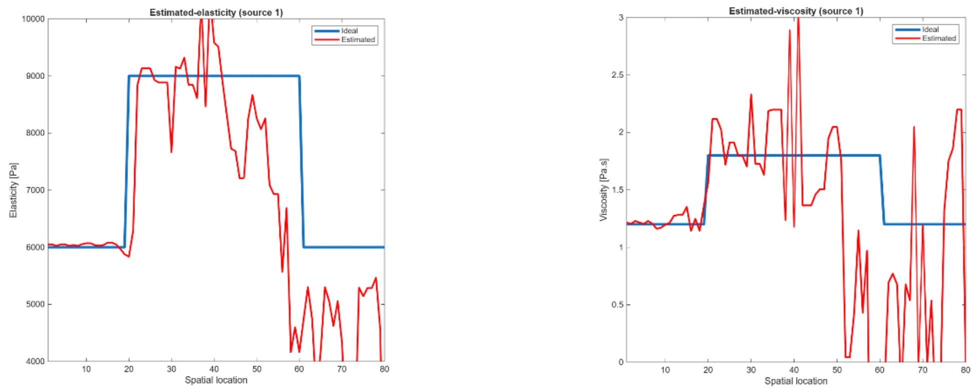

Figure 3.10: Elasticity and viscosity profiles along line 40]

Source at position 2

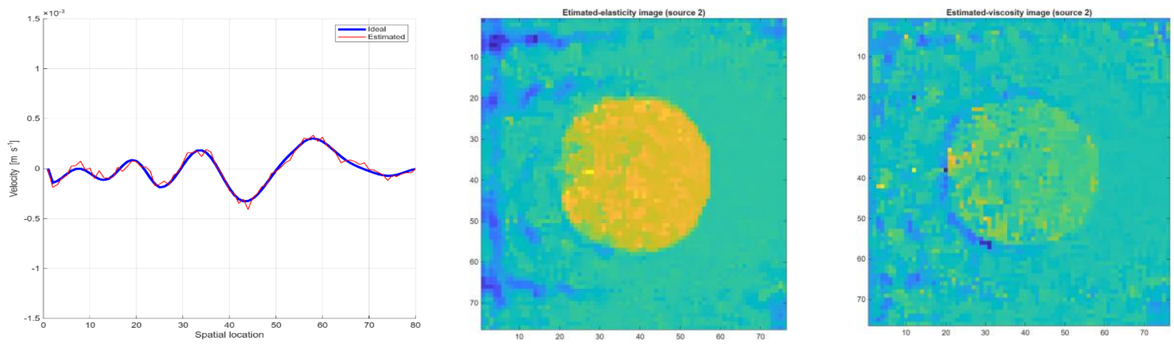

Figure 3.11: Estimated elasticity and viscosity images at position 2

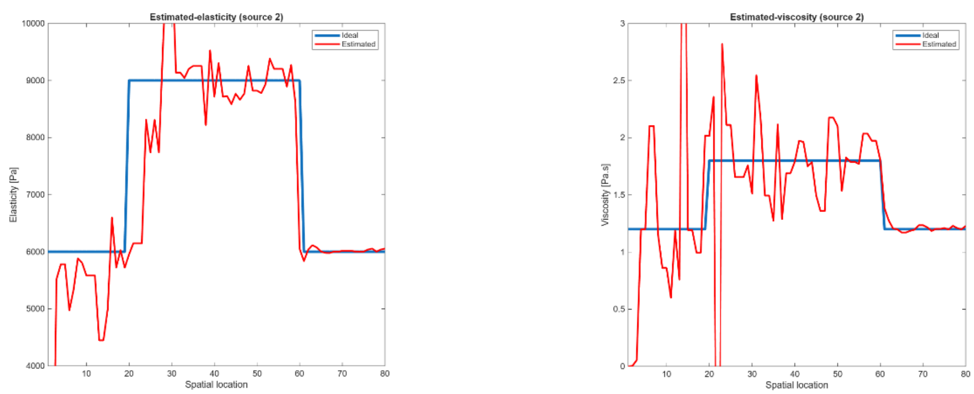

Figure 3.12: Elasticity and viscosity profiles along line 40

Combination of sources 1 and 2

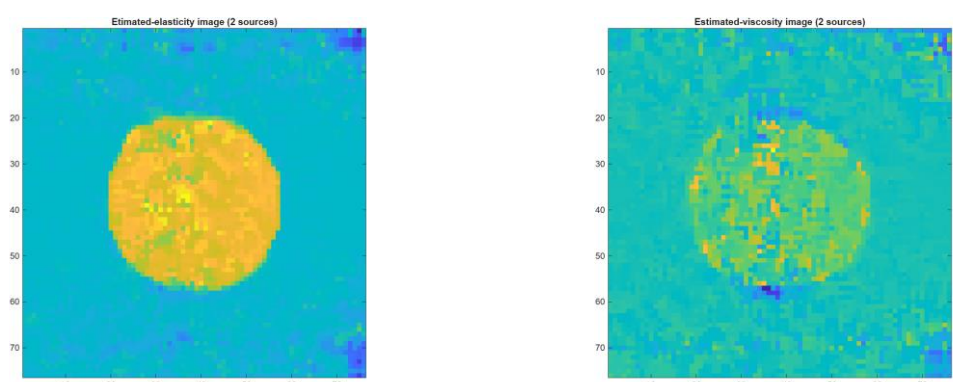

Figure 3.13: Combined elasticity and viscosity images

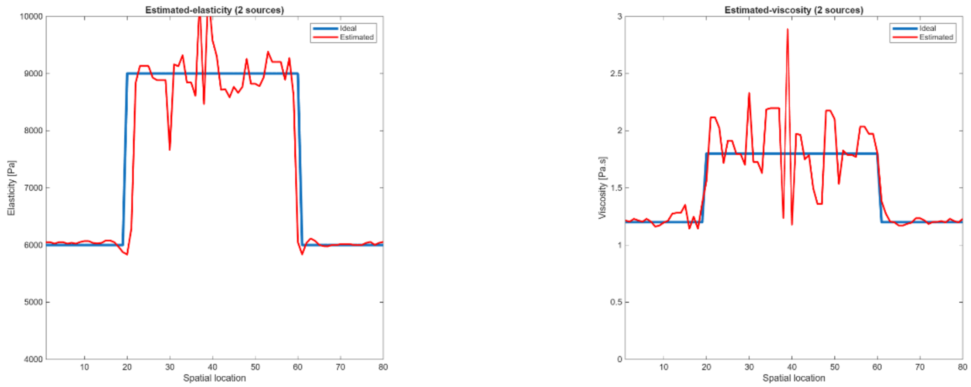

Figure 3.14: Combined elasticity and viscosity profiles

3.4. The Q-index

$$Q = 4\sigma_{xy} \cdot \bar{x} \cdot \bar{y} / [(\sigma^2_x + \sigma^2_y) \cdot (\bar{x}^2 + \bar{y}^2)] \qquad (3.1)$$

Table 3.2: Q-index values for elasticity and viscosity images

SNR (dB)	Q_el_s1	Q_el_s2	Q_el_cb	Q_vi_s1	Q_vi_s2	Q_vi_cb
19	0.662	0.769	0.927	0.198	0.240	0.532
21	0.725	0.823	0.946	0.227	0.309	0.622
23	0.821	0.847	0.954	0.336	0.433	0.709
25	0.848	0.897	0.961	0.375	0.453	0.798
27	0.895	0.913	0.963	0.521	0.547	0.861
29	0.919	0.935	0.965	0.582	0.609	0.870

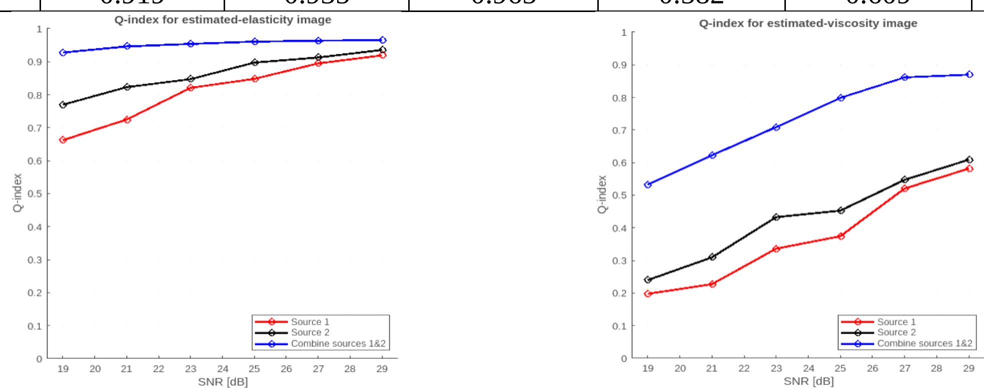

Figure 3.15: Q-index for the estimated elasticity and viscosity images

3.5. The RMSE (Root Mean Square Error)

R_el_s1, R_el_s2, R_el_cb denote the RMSE of the elasticity image at source position 1, source position 2, and the combined image, respectively. Similarly, R_vi_s1, R_vi_s2, R_vi_cb denote the RMSE of the viscosity image at source position 1, source position 2, and the combined image, respectively.

Table 3.3: RMSE of elasticity and viscosity images

SNR (dB)	R_el_s1	R_el_s2	R_el_cb	R_vi_s1	R_vi_s2	R_vi_cb

19	1456.4	1087.7	490.6	0.6971	0.5911	0.3269
21	1211.0	876.9	410.1	0.6013	0.5039	0.2690
23	886.5	794.1	377.7	0.4751	0.3996	0.2176
25	793.1	613.5	345.8	0.4376	0.3688	0.1743
27	624.2	548.8	332.2	0.3343	0.3133	0.1425
29	527.1	459.6	323.0	0.2911	0.2738	0.1349

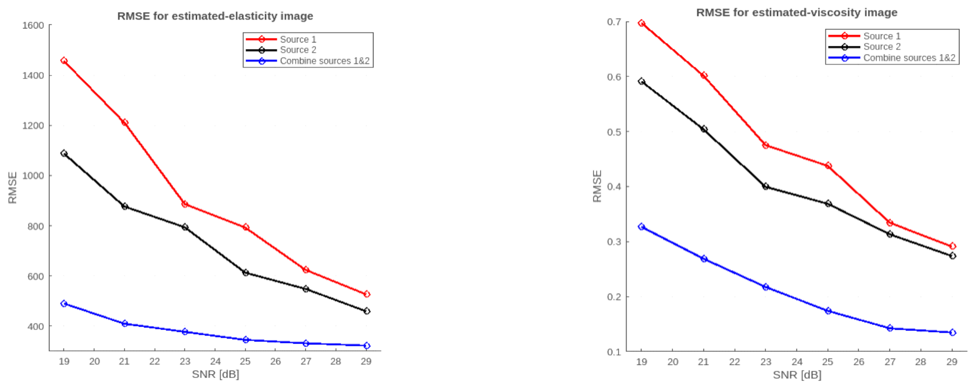

Figure 3.16: RMSE for the estimated elasticity and viscosity images

3.6. Comparison with the study by Xufei Chen

Xufei Chen [103] proposed a 3D multi-resolution convolutional neural network (MRCNN) to improve the SNR of shear-wave signals in shear-wave elastography. The method uses high-quality training data generated from multiple plane-wave compounding acquisitions to denoise and enhance elasticity image quality, thereby increasing the SNR and improving the CNR and RMSE indices. However, this approach requires a complex training procedure and substantial computational resources, and carries the risk of over-smoothing or reconstructing artefactual signal details. Furthermore, the study focuses mainly on elasticity images and does not evaluate tissue viscosity.

In contrast, the method proposed by the candidate uses two mechanical excitation sources from a vibrating needle to generate shear waves, allowing flexible control of the position and intensity of excitation while improving signal quality in deep-tissue regions. Combined with directional, LMS, and median filters, the proposed method suppresses noise directly on the velocity signal without requiring training data. In particular, the method enables the simultaneous reconstruction of elasticity and viscosity images, providing a more comprehensive characterisation of the viscoelastic properties of biological tissue.

Conclusion of Chapter 3

In this study, the candidate proposes a method using two excitation sources to improve viscoelastic image quality, particularly in deep-tissue regions. Although the processing time is longer than that of a single-source method, the total simulation time remains acceptable (approximately 3 minutes on a personal computer and 1 minute on MATLAB Online). Qualitative and quantitative results show that images combined from the two excitation sources are of clearly higher quality than those obtained from each source individually. At SNR = 27 dB, the combined viscosity image achieves RMSE = 0.1425, substantially lower than the values 0.3133 and 0.3343 obtained from the two single sources. Similarly, the combined elasticity image achieves RMSE = 332.21, a clear improvement over 548.77 and 624.25. The Q-index also increases substantially, with the elasticity image reaching 0.963 and the viscosity image 0.861. These results confirm the effectiveness of the multi-point excitation method in enhancing the quality of viscoelastic images.

CONCLUSIONS AND FUTURE WORK

CONCLUSIONS

In this dissertation, the candidate has investigated and developed methods for estimating the complex shear modulus of soft tissue based on the shear-wave velocity field in ultrasound elastography. The central focus of the dissertation is to address the limitations commonly encountered in the reconstruction of viscoelastic images, particularly the effects of measurement noise, reflected waves, and shear-wave energy attenuation in inhomogeneous tissue environments and deep-tissue regions.

Based on shear-wave propagation modelling and numerical simulation using the finite-difference time-domain method, the dissertation has developed and evaluated signal-processing methods to improve the stability of Helmholtz inversion in the estimation of the complex shear modulus. The simulation results show that the proposed methods substantially improve viscoelastic image quality and reduce the estimation error of tissue mechanical parameters under various noise conditions. Through the simulation scenarios, the dissertation has clarified the relationship between the quality of the shear-wave velocity, the signal-processing pipeline, and the reliability of the resulting viscoelastic images. These results demonstrate that the proposed approach can effectively overcome the limitations of conventional estimation methods, particularly in complex tissue environments and deep-survey regions.

Scientific contributions of the dissertation

Contribution 1: Proposing a framework for more stable complex-shear-modulus estimation in inhomogeneous tissue environments

The dissertation proposes a signal-processing and complex-shear-modulus estimation framework based on algebraic Helmholtz inversion (AHI), in which the characteristic noise types in ultrasound elastography — random noise, speckle noise, and reflection noise — are processed sequentially according to the properties of each type. The novelty of this contribution lies not in any individual processing technique, but in the sequential combination of filters matched to each noise type, together with the direct evaluation of the impact of this processing pipeline on the complex shear modulus image rather than only on the shear-wave velocity signal. This approach reduces error propagation from the velocity signal to the viscoelastic image, thereby enhancing the stability and reliability of the complex shear modulus image in inhomogeneous tissue environments.

Contribution 2: Improving viscoelastic image quality in deep-tissue regions through multi-point excitation

The dissertation proposes a multi-point excitation model to overcome depth-dependent shear-wave energy attenuation, which is the primary cause of decreased signal-to-noise ratio and biased complex-shear-modulus estimation in regions far from the excitation source. The novelty of this contribution lies in the application of multi-point excitation in the context of simultaneous estimation of elasticity and viscosity, combined with the noise-processing pipeline and Helmholtz inversion, to directly evaluate the improvement in the complex shear modulus image rather than focusing only on the velocity signal. The simulation results show that the proposed method clearly improves viscoelastic image quality in deep-tissue regions, as quantitatively demonstrated by the RMSE and Q-index.

General assessment

The contributions of the dissertation do not aim to construct an entirely new physical model. Rather, they focus on the integration and optimisation of existing physical, mathematical, and signal-processing tools to enhance the accuracy and stability of viscoelastic images under complex tissue conditions. The results obtained demonstrate that the dissertation has scientific value and practical application potential in the field of ultrasound elastography.

LIMITATIONS OF THE STUDY

Although the proposed methods have achieved positive results in improving viscoelastic image quality, the dissertation still has certain limitations.

First, the results in the dissertation were obtained on simulation data under controlled noise conditions. This means that the method has not yet been validated in real environments, where additional complex factors such as physiological noise, tissue anisotropy, and instrument-to-instrument variability are present. Consequently, the accuracy of the proposed method under realistic conditions should be further evaluated on physical phantoms and clinical data in subsequent studies.

Second, the shear-wave propagation model and the complex-shear-modulus estimation procedure are implemented in two-dimensional space. This is a simplifying assumption compared with the three-dimensional structure of real biological tissue, particularly when tumours exhibit complex morphology and uneven spatial distribution. Specifically, the 2D model neglects the shear-wave energy component along the third axis and therefore does not fully capture amplitude attenuation in real space. Moreover, reflection and scattering at tissue boundaries in 3D are considerably more complex than under the planar assumption in 2D, which may affect the accuracy of viscoelastic images in real applications. Extending the model to 3D, in which the shear-wave velocity field is estimated along all three spatial directions, is identified as a future research direction.

Third, although the two-point excitation method improves the SNR in deep-tissue regions, sequential excitation increases acquisition time and requires high precision in source positioning; furthermore, the method is susceptible to tissue motion, which reduces the reliability of results under realistic clinical conditions. To mitigate these issues, several practical solutions can be applied: first, optimising the timing between excitations to reduce the waiting period between measurements; second, leveraging the B-mode image already available on the ultrasound device to visually assist excitation-source positioning prior to measurement; third, synchronising the measurement time with a stable phase of the respiratory cycle to limit the influence of tissue motion on the acquired signal. These solutions do not require hardware modification and are highly feasible in clinical settings; they will be investigated and evaluated in the next phase of the research.

FUTURE WORK

Although the dissertation has achieved certain results in improving the quality of viscoelastic ultrasound images through complex-shear-modulus estimation of soft tissue, several issues remain to be further investigated and refined to enhance the generality and practical applicability of the proposed method. The following research directions are recommended:

Extension to three-dimensional (3D) problems:

Develop a measurement and estimation model for shear-wave velocity along three spatial directions (x, y, z), enabling the reconstruction of volumetric complex-shear-modulus images. This direction allows a more comprehensive description of the spatial structure of biological tissue, as well as the shape and volume of tumours, thereby enhancing diagnostic value compared with conventional 2D images.

Validation on experimental and clinical data:

Apply the proposed method to experimental data sets, including phantom and clinical data, in order to evaluate its reliability and ability to differentiate healthy and diseased tissue under real measurement conditions. Furthermore, comparison between simulation results and real data will help refine the model assumptions and adjust signal-processing parameters to match the characteristics of different ultrasound systems.

Enhanced noise-suppression capability:

Investigate the combination of additional excitation source types, beyond the current mechanical excitation, to improve the quality of the acquired shear-wave field. Combining different excitation sources with signal-processing filters (LMS, median, directional) may further enhance noise suppression, particularly in deep-tissue regions and inhomogeneous tissue environments containing tumours.

LIST OF PUBLICATIONS RELATED TO THE DISSERTATION

[CT1]	Quang-Hai Luong, **Nguyen Sy Hiep**, Duc-Nghia Tran, Duc-Tan Tran, "Improving tissue elastography image quality using multi-position shear wave stimulation and LMS/AHI-based filtering", Results in Engineering, Volume 27, 2025, 107012, ISSN 2590-1230, https://doi.org/10.1016/j.rineng.2025.107012. **(Tạp chí Q1)**
[CT2]	**N. Sy Hiep,** D.-N. Tran, V. K. Solanki, D.-T. Tran, and Q. H. Luong, "Enhancing 2D elasticity and viscosity images: A denoising approach for reflected and random noise removal", Ingeniería Solidaria, vol. 21, no. 3, pp. 1–18, Feb. 2026, doi: 10.16925/2357-6014.2025.03.02. (**ESCI)**
[CT3]	**Nguyen Sy Hiep**, Luong Quang Hai, Tran Duc Tan, Pham Van Tang, Tran Duc Nghia*, Improving the quality of deep-tissue elastography imaging: A Kelvin–Voigt model-based and multi-point denoising approach, Journal of Military Science and Technology, vol. 110 (2026), pp. 34-44, Apr. 2026, DOI: https://doi.org/10.54939/1859-1043.j.mst.110.2026.34-44
[CT4]	**Hiep, N.S**., Hai, L.Q., Nghia, T.D., Tan, T.D. (2023). Evaluating the Improvement in Shear Wave Speed Estimation Affected by Reflections in Tissue. In: Nguyen, T.D.L., Verdú, E., Le, A.N., Ganzha, M. (eds) Intelligent Systems and Networks. ICISN 2023. Lecture Notes in Networks and Systems, vol 752. Springer, Singapore. https://doi.org/10.1007/978-981-99-4725-6_54 **(Scopus)**
[CT5]	**Hiep, N.S**., Nghia, T.D., Hai, L.Q., Thuong, V.T., Prakash, K.B., Tan, T.D. (2024). Enhancing Shear Wave Estimation Through Directional and Kalman Filters for Noise Reduction. In: E. Balas, V., Prakash, K.B., Varma, G.P.S. (eds) Proceedings of the International Conference on Internet of Everything and Quantum Information Processing. IEQIP 2023. Lecture Notes in Networks and Systems, vol 1029. Springer, Cham. https://doi.org/10.1007/978-3-031-61929-8_24 **(Scopus)**
[CT6]	Q. H. Luong, **S. -H. Nguyen**, D. -N. Tran, C. M. Nguyen and D. -T. Tran, "Viscoelastic Estimation of Soft Tissue in the Presence of Gaussian and Reflection Noises Impacting Shear Wave Propagation," 2023 12th International Conference on Control, Automation and Information Sciences (ICCAIS), Hanoi, Vietnam, 2023, pp. 622-627, doi: 10.1109/ICCAIS59597.2023.10382326. **(Scopus)**
[CT7]	Q. H. Luong, D. -N. Tran, **N. S. Hiep**, L. S. Cong and D. -T. Tran, "Enhancing Shear Wave Propagation Analysis in Tissue with Directional Filtering of Reflected Waves," 2024 Asia Pacific Signal and Information Processing Association Annual Summit and Conference (APSIPA ASC), Macau, Macao, 2024, pp. 1-6, doi: 10.1109/APSIPAASC63619.2025.10848844. **(Scopus)**